WILEY-VCH

DOI: 10.1002/((please add manuscript number))
Article type: Full Paper

Defect Dynamics in Proton Irradiated $CH_3NH_3PbI_3$ Perovskite Solar Cells

Viktor V. Brus[*], *Felix Lang, Jürgen Bundesmann, Sophie Seidel, Andrea Denker, Bernd Rech, Giovanni Landi, Heinrich C Neitzert, Jörg Rappich and Norbert H. Nickel*[*]

Dr. V.V. Brus, F. Lang, Prof. Dr. B. Rech, Dr. J. Rappich, Prof. Dr. N. H. Nickel,
Helmholtz-Zentrum Berlin für Materialien und Energie GmbH, Institut für Silizium Photovoltaik, Kekuléstr. 5, 12489 Berlin, Germany.
[*]Emails: victor.brus@helmholtz-berlin.de, nickel@helmholtz-berlin.de

Dr. V.V. Brus
Department of Electronics and Energy Engineering, Chernivtsi National University, Kotsubynskiy 2, 58002 Chernivtsi, Ukraine

J. Bundesmann, S. Seidel, Dr. A. Denker
Helmholtz-Zentrum Berlin für Materialien und Energie GmbH, Protons for Therapy, Hahn-Meitner Platz 1, 14109 Berlin, Germany

Dr. G. Landi, Prof. Dr. H. C. Neitzert
Department of Industrial Engineering (DIIn), Salerno University, Via Giovanni Paolo II 132, 84084 Fisciano (SA), Italy

Keywords: perovskite, photo-degradation, proton irradiation, compensation.

Abstract

Perovskite solar cells have been shown to be of extraordinary radiation hardness, considering high energetic (68MeV) proton irradiation with doses up to 10^{13} p cm^{-2}. Here electrical and photoelectrical properties of perovskite solar cells with and without proton irradiation were analyzed in details. Our results reveal that proton irradiation improves the open circuit voltage, fill factor and recombination lifetime of photo-generated charge carriers in perovskite solar cells. These enhancements are mainly a result of the lower non-radiative recombination losses in the proton irradiated devices. The proton treatment creates shallow traps, which may be associated with the proton induced point defects due to the displacements of atoms in the inorganic Pb-I framework, which act as unintentional doping sources and

partially compensate deep traps originated from the photo-degradation of methylammonium molecules.

1. Introduction

A rapid growth of different scientific and commercial space programs makes the fabrication of solar cells for space applications an important segment of the nowadays photovoltaic industry. Space applications of solar cells necessitate a number of strict requirements such as: high efficiency, low weight and high radiation hardness.[1-3] In space solar cells are exposed to a flow of high energy particles (electrons, protons and α-particles), which originate from the solar wind. High energy particles generate defects in the crystalline lattice of semiconductors used in solar cells. Radiation induced defects give rise to localized states within the band gap and hence increase recombination losses in solar cells. Therefore, only materials with an elevated radiation resistance can be used for solar cells that are employed in space.

Moreover, there are huge territories with high radioactive pollution that are spread all over the world. The largest radioactively polluted zones are: the Chernobyl Exclusion Zone in Ukraine and Belarus (~2600 km^2), the Fukushima Exclusion Zone in Japan (~1300 km^2), the Nevada Nuclear Test Site in the USA (~3500 km^2) and the Semipalatinsk Nuclear Test Site in Kazakhstan (~18000 km^2). These huge territories, surrounded by heavily populated regions, are completely excluded from any economic activities of their countries for centuries. The installment of solar panels does not require capital constructions, which are forbidden in the mentioned zones. Thus, the territories with their already existing highly developed electric-power infrastructures could be reintegrated into the economic life and energy systems of their countries. However, besides standard requirements such as low cost and high efficiency the solar cells to be installed in radioactively polluted zones should also possess a high radiation hardness in order to warrant reliable and long-term operation.

Hybrid organic-inorganic methylammonium lead tri-halide perovskites continuously show unique features, which considerably broaden the field of their possible applications: high efficient solar cells[4, 5], photo-capacitors and piezoelectric sensors[6], memristors[7], etc. Perovskite solar cells have reached an amazing increase in power conversion efficiency η, during last few years. Recently, a value beyond η = 22% was reported.[8] The superior efficiency in combination with thin-film architecture and low-cost fabrication techniques make perovskite solar cells very attractive. Taking into account the large variety of interesting properties of perovskites, it can be assumed that this class of material has still many unknown features that merit further investigations.

Recently, we have shown a high radiation hardness and a self-healing effect in perovskite solar cells by *in-situ* measurements during high-energy proton bombardment.[9] The radiation hardness of perovskite solar-cells was established to be about three orders of magnitude higher than that of conventional crystalline silicon (c-Si) solar cells.[10] A unique combination of the high radiation hardness with the high efficiency, the low weight thin-film architecture and the low-cost manufacturing make regular perovskite solar cells and high efficiency perovskite/$Cu_2InGaSe_4$ (CIGS) tandem solar cells attractive for operation in radioactively polluted zones and for space applications. However, the physics of proton induced changes in perovskite solar cells and their relationship with photoelectric parameters is still unknown and has to be investigated in details. Providing insight into this question is exceedingly complicated because of the intrinsic aging and photo-degradation processes that are characteristic for perovskite solar cells. Therefore, the aim of this paper is to distinguish between the photo-degradation and proton induced changes in perovskite solar cells and understand how they are related and influence on each other. For this reason a detailed quantitative analysis of the perovskite solar cells with and without high energy proton treatment was carried out under the same illumination conditions. DC and AC electrical characteristics of the devices in the dark and under illumination are presented and compared

to address differences in their device physics and operation characteristics. The obtained experimental results will be discussed in terms of models developed for simultaneous photo-degradation and proton irradiation treatment.

2. Experimental results

Two batches of the same typical perovskite solar cells (referred as cell A and cell B, with three devices in each) were prepared following the layer sequence glass/ITO/PEDOT:PSS/$CH_3NH_3PbI_3$/$PC_{61}BM$/BCB/Ag (**Figure 1a**). This sequence has the advantage that the hysteresis in the J-V curves is small. The solar cells were encapsulated in dry nitrogen atmosphere (O_2< 0.1 ppm and H_2O < 0.1 ppm) using two component epoxy. Characterization under AM 1.5, as shown in **Figure 1b**, revealed very close initial photoelectrical parameters for both batches of as-prepared solar cells. More detail compression of the dark and light J-V characteristics of the perovskite solar cells as well as the reproducibility of the effect of the light and the simultaneous light and proton irradiation treatments can be found in the Supporting Information.

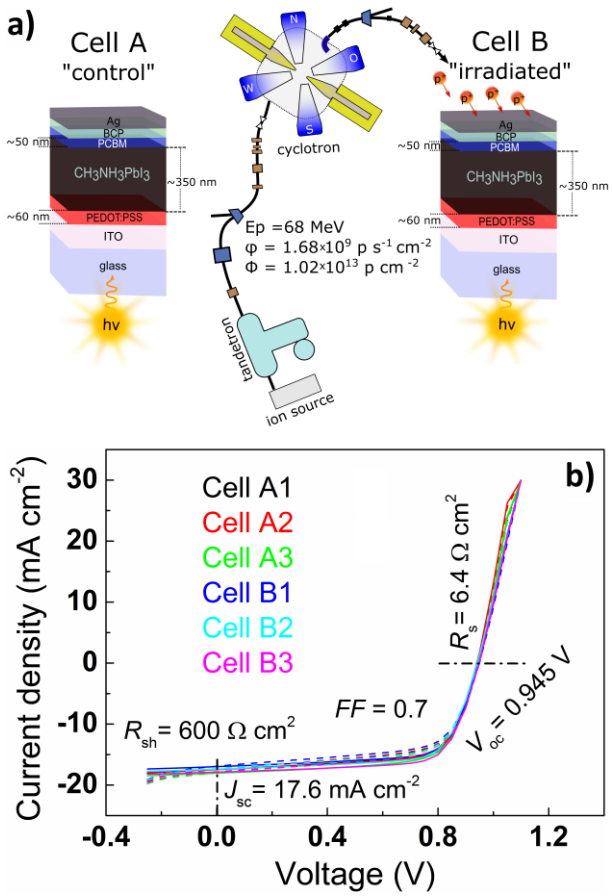

Figure 1. **a)** Schematic representation of the light treatment of cell A and the simultaneous light and proton irradiation treatments of cell B. **b)** Initial J-V curves of the as-prepared perovskite solar cells under the 1.5 AM illumination condition. The average efficiency of the solar cells under investigation is 11.6 %. Dashed lines show the forward scan direction and solid lines show the reverse scan direction.

Cell A and cell B were treated by white light with the intensity of 100 mW cm^{-2} for 100 min. Cell B was also simultaneously exposed to high energy (68 MeV) protons with a constant flux $\varphi = 1.68\times10^{9}$ p cm^{-2} s^{-1} until the total dose of 1.02×10^{13} p cm^{-2} was reached after 100 min. The solar cells were subsequently encased in lead containers for 10 days to allow the induced radioactivity to decline. Afterwards, DC and AC electrical and photoelectrical characteristics of proton untreated and proton irradiated solar cells were measured. Hereafter, "control" will

be referred to the proton untreated cell A and "irradiated" will refer to the proton irradiated cell B.

2.1. DC and AC characteristics in the dark

J-V characteristics

Figure 2a shows J-V characteristics of the control and irradiated solar cells that were measured in the dark at room temperature after 10 days of storage.

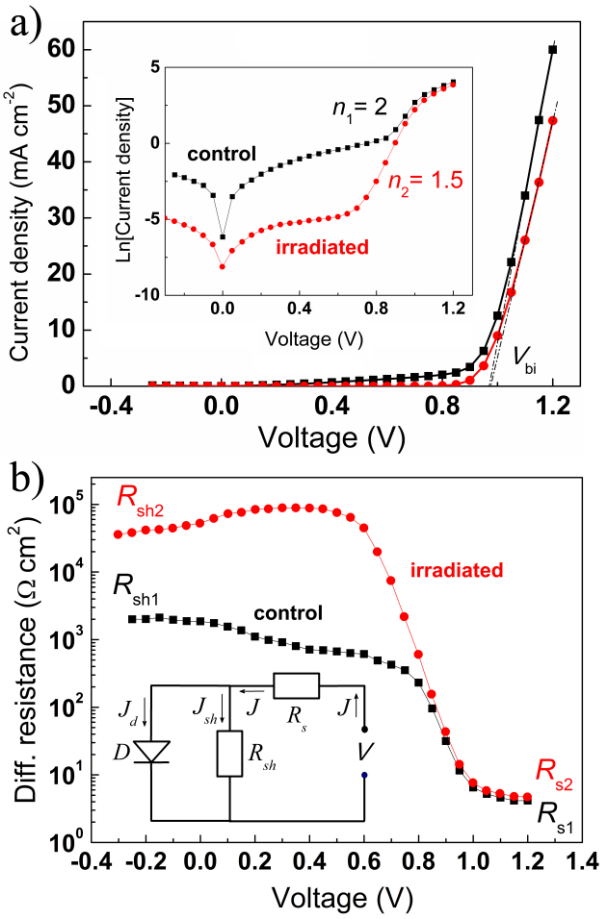

Figure 2. a) J-V curves of the control (black rectangles) and irradiated (red circles) solar cells. V_{bi} denotes the build-in voltage. The inset shows a semi-logarithmic plot of the data. **b)** Differential resistance as a function of the applied bias V, for the control and irradiated solar cells. R_{s1} and R_{s2} denote the series resistance while R_{sh1} and R_{sh2} denote the shunt resistance of the control and irradiated solar cells. The inset shows the DC equivalent circuit diagram. Here, J_d is the diode current, J_{sh} is the shunt current, D is the rectifying junction.

The value of the built-in voltage V_{bi} can be estimated by extrapolating the linear parts of the J-V curves to $J = 0$.[11] Both devices show almost the same built-in voltage of $V_{bi} = 0.97$ V. This indicates that the dose of 10^{13} p cm^{-2} does not change the work functions of the electron and hole collecting electrodes. However, a large difference in the leakage current can be seen in the semi-logarithmic plot (see inset of Figure 2a). Surprisingly, the leakage current of the irradiated solar cell is much smaller compared to that of the control solar cell. The ideality coefficient of the irradiated solar cell $n_2 = 1.5$ is larger than unity that indicates the presence of the trap-assisted recombination mechanism besides the direct free carrier recombination.[12] Deep traps act as non-radiative recombination centers according to the Shockley-Read-Hall (SRH) statistics and partially participate in the dark current.[13] The ideality coefficient of the control solar cell amounts to $n_1 = 2$. This means that the majority of injected charge carriers recombine within the active layer via deep traps. This current transport mechanism is quantitatively described in the scope of the Sah–Noyce–Shockley model, originally developed for p-n homojunctions and later modified for heterojunctions with deep traps.[14, 15]

The voltage dependence of differential resistance $R_{diff} = \Delta V/\Delta J$ is shown in **Figure 2b**. The series resistance R_s can be determined by the extrapolation of the saturated part at large forward bias toward the interception with the resistance axis. It is seen that the series resistance is almost the same for both devices and thus, it can be concluded that the hole and electron collecting contacts were not affected by proton irradiation. The shunt resistance R_{sh} is determined by the value of R_{diff} in the vicinity of zero bias. It is seen that $R_{sh1} << R_{sh2}$ because the control solar cell possesses a much larger leakage current in comparison to the irradiated solar cell. The leakage channel which significantly reduces the shunt resistance R_{sh1} is caused by the high-rate SRH recombination of injected charge carriers within the active layer of the control device since its ideality coefficient $n_1 = 2$.

Based on the presented dark DC characteristics it appears that the rate of the undesirable SRH recombination of injected charge carriers within the perovskite layer is reduced after the proton irradiation treatment. The following capacitance and photo-electrical experimental data will provide additional information about proton-induced changes in the irradiated solar cell.

Capacitance characteristics

The measured impedance spectra of the control and irradiated solar cells at different biases in the dark were corrected by the effect of the series resistance R_s and the parasitic inductance of the connecting wires $L = 10^{-6}$ H to calculate the actual capacitance C_{cor} using the following equation[16, 17]

$$C_{cor} = -\frac{1}{\omega}\left[\frac{Z'' - \omega L}{(Z' - R_s)^2 + (Z'' - \omega L)^2}\right]. \quad (1)$$

Here, Z' and Z'' are the real and imaginary components of the measured impedance, respectively, and $\omega = 2\pi f$ is the angular frequency of the small amplitude (10 mV) AC signal. The importance of the mentioned corrections is clearly seen in **Figure 3a**, where the measured and corrected capacitance spectra are compared. The parasitic contributions of R_s and L on the measured capacitance become significant at frequencies $f > 10^5$ Hz.

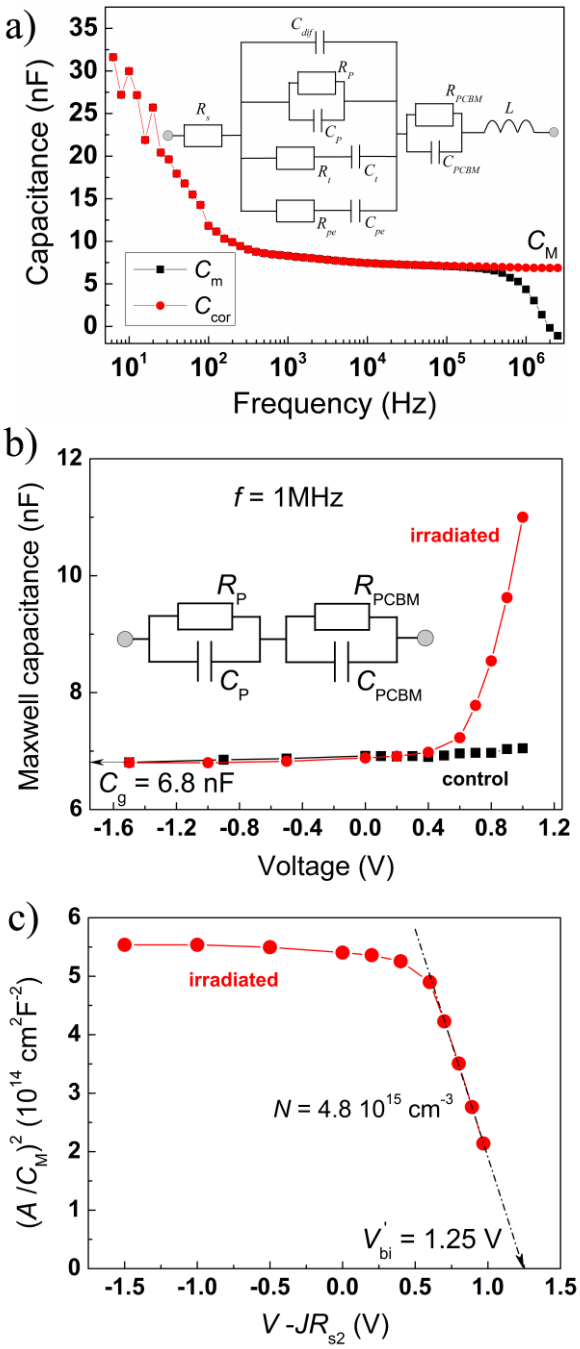

Figure 3. a) The measured C_m, and corrected C_{corr} capacitance spectra, of the control solar cell at zero bias in the dark. The inset shows an equivalent circuit of the perovskite solar cells in first approximation, were C_{dif} is the diffusion capacitance originated from the injected charge carriers, R_P and C_P are the resistance and capacitance, respectively, of the perovskite layer; R_{PCBM} and C_{PCBM} are the resistance and capacitance, respectively, of the PCBM layer; R_t and C_t are the resistance and capacitance, respectively, associated with the charging and discharging traps; R_{pe} and C_{pe} are the resistance and capacitance, respectively, associated with

the polarization effects; C_M is the Maxwell displacement capacitance. **b)** C_M vs. applied bias in the dark at room temperature, C_g is the geometric capacitance. The inset shows a high frequency equivalent circuit of the perovskite solar cells after corrections by R_s and L. **c)** Mott-Schottky plot for the irradiated solar cell. N is the density of uncompensated doping sources.

From Figure 3a we can conclude that the low frequency capacitance is much larger than that at high frequency. The spectral dependence can be explained by considering different processes, which may contribute to the capacitance within a wide range of frequencies (see inset in Figure 3a). If a low frequency AC signal is applied to a perovskite solar cell a number of physical processes can follow the AC signal and contribute to the measured capacitance. These processes comprise injection of free charge carriers, charging and discharging of defect states due to Fermi level oscillations, ions movement, polarization effects, and Maxwell displacement currents.[6, 16-19] The capacitance originating from the Maxwell displacement currents is frequency independent up to ~1 GHz which is far beyond the spectral range used in our study.[17, 20] However, all other mechanisms strongly depend on frequency since their physical processes cannot follow a high frequency AC signal. Therefore, the large low-frequency capacitance decreases with the increase of frequency and saturates at a level, which is determined by the frequency independent Maxwell displacement capacitance (C_M) (Figure 3a). This frequency independent capacitance is determined by the thickness of the depleted region. C_M is voltage independent if the active layer of the solar cells is completely depleted and does not change with the applied bias. C_M is equal to the geometric capacitance between two electrodes $C_g = \varepsilon\varepsilon_0 A/d$, where ε is the dielectric constant, ε_0 is the permittivity of free space, A is the area of the electrodes, and d is the distance between the electrodes. However, if the material of an active layer is doped the depletion region may be narrower in comparison to the total thickness of the active layer. In this case the width of the depletion layer can be

modulated by the applied bias and thus C_M will become voltage dependent according to the Mott-Schottky model:[13]

$$C_M = A\sqrt{\frac{\varepsilon\varepsilon_0 qN}{2(V_{bi}-V_{cor})}}. \quad (2)$$

Here N is the density of uncompensated donors or acceptors and $V_{cor} = V\text{-}JR_s$ is the applied bias corrected by the voltage drop over the series resistance.

Figure 3b shows the voltage dependence of the high frequency (1 MHz) corrected capacitance (C_M) of the control and irradiated solar cells. C_M of both devices saturates at reverse and small forward biases. All charge carriers are extracted from the system at reverse bias and the saturated C_M is the geometric capacitance C_g between the electrodes and amounts to 6.8 nF. The high frequency equivalent circuit consists of two capacitors connected in series (see inset in Figure 3b). $C_{PCBM} = \varepsilon_{PCBM}\varepsilon_0 A/d_{PCBM}$ is the geometric capacitance of the PCBM film (d_{PCBM} = 45 nm) and $C_P = \varepsilon_P\varepsilon_0 A/d_P$ is the geometric capacitance of the perovskite film (d_P = 350 nm). The dielectric constant of PCBM amounts to ε_{PCBM} = 3.9[21] and the dielectric constant of perovskite ε_P can be calculated from the following equation:

$$\varepsilon_P = \frac{\left[\frac{C_g C_{PCBM}}{C_{PCBM}-C_g}\right] d_P}{\varepsilon_0 A}. \quad (3)$$

Equation 3, which takes into account the capacitance contribution from the PCBM layer, yields ε_P = 38. The large value of ε_P results from the organic-inorganic hybridization of lead halide via the interaction with the methylammonium framework.[22] In the following, this value will be used for our further analysis.

The dielectric constants were not changed by the proton treatment since the geometric capacitance of both devices is the same. However, the control and irradiated solar cells behave differently at a large forward bias of $V_{cor} > 0.3$ V. The capacitance of the control solar cell is almost independent on voltage. This means that the perovskite material is close to

intrinsic since the active layer is totally depleted even at large forward bias. The irradiated solar cell shows a strong voltage dependence of its capacitance and the proton treated perovskite layer behaves as a doped semiconductor.

Figure 3c shows the Mott-Schottky plot of the irradiated solar cell. The linear dependence of $(A/C_M)^2$ vs. corrected voltage at large forward bias points to a uniform distribution of doping sources within the perovskite layer. This fact is in good agreement with the high energy of the protons (68 MeV), which provide a uniform treatment of the volume of thin films.[9] The built in voltage $V_{bi}' = 1.25$ V is determined by the extrapolation toward the interception with the voltage axis (see Equation 1). The density of uncompensated doping sources N was calculated from the slope of the linear dependence according to[13]

$$N = \frac{2}{q\varepsilon_P\varepsilon_0\left[\frac{\Delta\left(A/C\right)^2}{\Delta\left(V - JR_{s2}\right)}\right]}. \quad (4)$$

N amounts to 4.8×10^{15} cm^{-3}. The discrepancy between the values of the built-in voltage determined from the J-V characteristics (V_{bi} = 0.97 V) and from the Mott-Schottky dependence ($V_{bi}' = 1.25$ V) can originate from the presence of an electrically charged interface according to the Donnelly-Milnes model, which describes capacitance characteristics of semiconductor heterojunctions in the presence of electrically charged interfaces, interface traps and dipoles.[23]

2.2. Photoelectrical properties

Figure 4a shows J-V curves of the control and irradiated solar cells under 100 mW/cm^2 of AM 1.5 illumination after 10 days in the storage cabinet. The control solar cell generates a larger J_{sc} than the irradiated solar cell. However, the open circuit voltage V_{oc} and the fill factor FF are improved after the proton treatment. As a result the efficiency of the

irradiated solar cell is higher. The difference between the photoelectric parameters of the control and irradiated solar cells will be discussed in details in this paragraph.

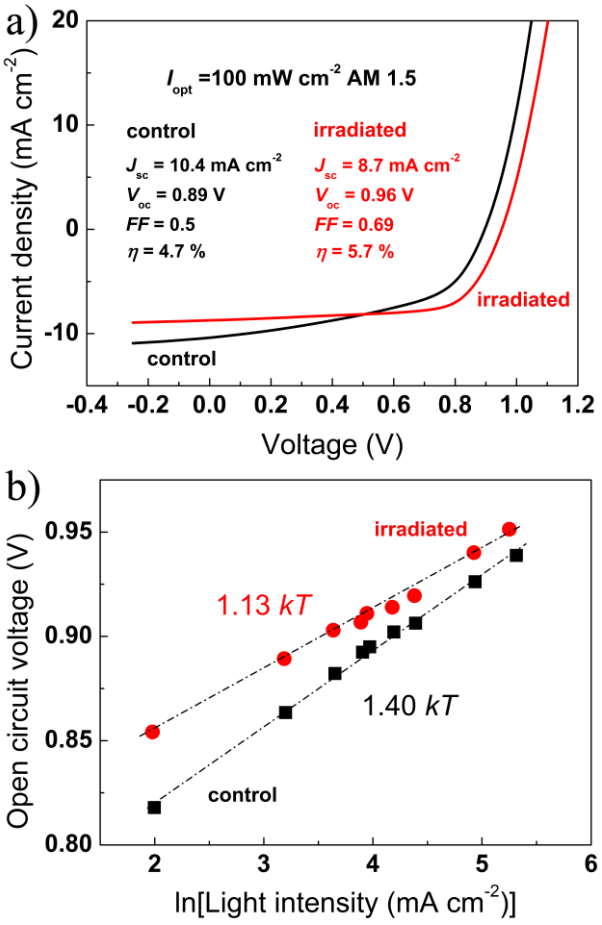

Figure 4. a) J-V characteristics of the control and irradiated solar cells under AM 1.5 illumination. The inset shows the photoelectric parameters J_{sc}, FF, V_{oc}, and η of both devices. **b)** Open circuit voltage vs. light intensity of the control and irradiated solar cells in the semi logarithmic scale. J-V curves, shown in Figure 4a, represent the reverse scan direction. The hysteresis of these J-V curves can be seen in the Supporting Information.

In our previous work[9] we have shown that the observed difference in J_{sc} originates purely from the proton induced darkening of the glass substrate[24] and has nothing to do with the proton damage of the perovskite active layer.

As seen from Figure 2a and 2b the irradiated solar cell possesses a slightly larger series resistance compared to the control solar cell. This means that the smaller fill factor of

the control solar cell (Figure 4a) is not caused by a large series resistance. Therefore, the difference in *FF* and V_{oc} between the two devices is caused by different recombination processes in these solar cells.

The open circuit voltage is directly related to and defined by recombination losses in solar cells. The light intensity dependence of V_{oc} has been utilized as a tool to determine dominant recombination mechanisms.[25, 26] Fitting the data in **Figure 4b** yields slopes S_1 = 1.13 kT/q and S_2 = 1.40 kT/q larger than kT/q. This indicates the presence of trap-assisted SRH recombination in both solar cells.[26, 27] However, the relative contribution of the SRH recombination to the total recombination is larger in the control solar cell than in the irradiated solar cell since $S_1 > S_2$, which is consistent with the ideality coefficients $n_1 > n_2 > 1$ (see inset in Figure 2a). Figure 4b leads to a non-trivial result, namely, that the high-energy proton irradiation decreases the undesirable non-radiative recombination losses via deep traps in the photo-degraded perovskite solar cells. This can be concluded from the fact that only defects with deep energy levels act as efficient recombination centers according to the SRH statistics.[13] Those deep traps are created during the photo-degradation of the perovskite.

Open-circuit voltage (V_{oc}) decay measurements were carried out to get insight into the understanding of V_{oc} and the dominant recombination processes in the control and irradiated solar cells. Under open-circuit conditions at high levels of excitation the decrease of the density of photo-generated charge carriers occurs by recombination. A fast switching LED light source with the intensity of 100 mW/cm^2 was used for the light excitation. **Figure 5a** shows V_{oc} decay curves for the control and irradiated solar cells.

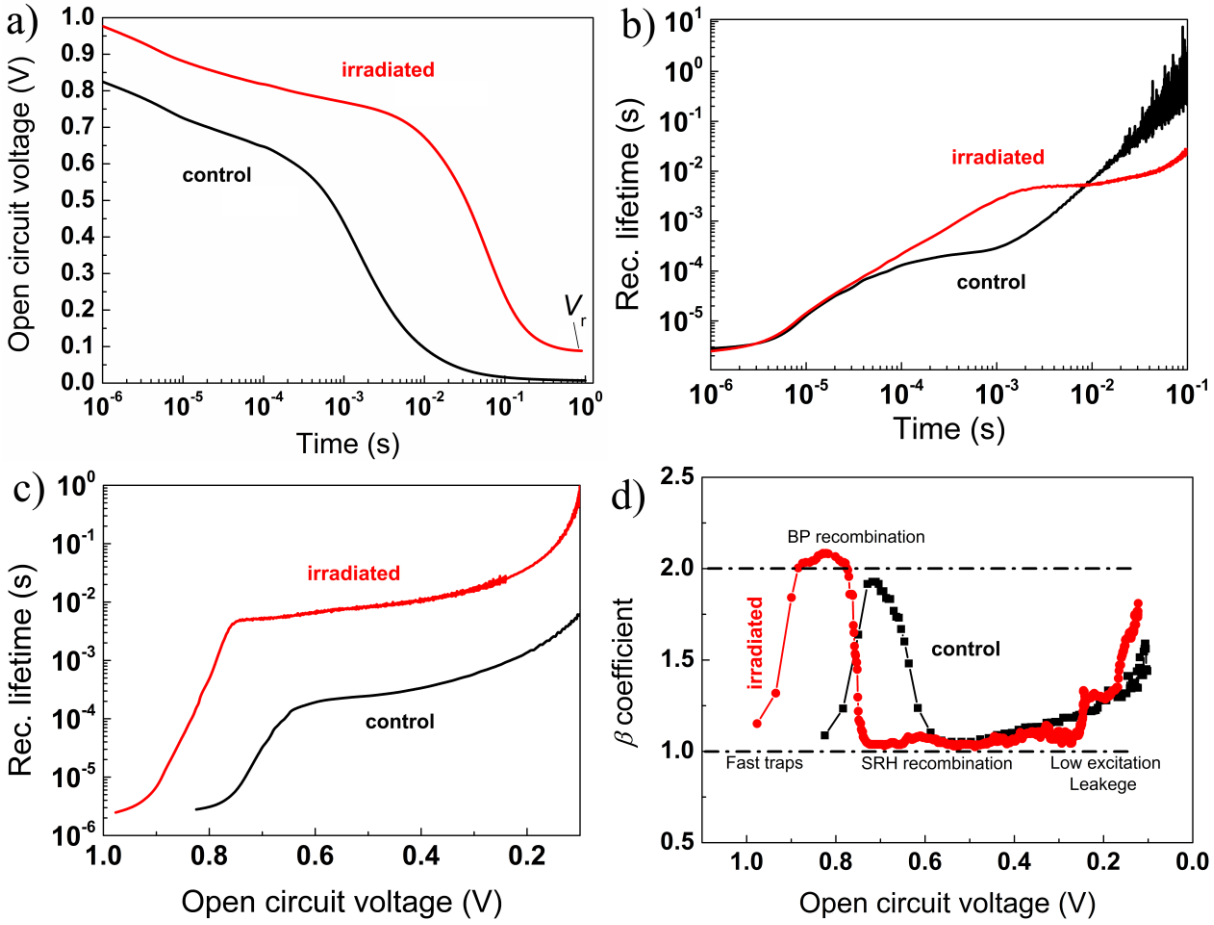

Figure 5. **a)** Open circuit voltage as a function of time at room temperature. The measurements were performed at room temperature (296 K). **b)** Recombination lifetime τ as a function time for the control and irradiated solar cells. **c)** Recombination lifetime τ as a function of V_{oc} for the control and irradiated solar cells. **d)** Effective recombination order as a function of V_{oc} for the control and irradiated solar cells.

V_{oc} of the control solar cell decays to zero within 1 s. On the other hand, the irradiated solar cell shows some residual voltage V_r after 1 s that slowly decays within a few minutes (not shown here). V_r may result from a prolonged release of charge carriers from traps, formed in the perovskite layer by the proton irradiation treatment.

For the V_{oc} decay measurements the net recombination rate $U(n)$ is given by[13]

$$U(n) = -\frac{dn}{dt} = -\frac{n}{\tau} = \gamma n^{\beta} \ , \qquad (5)$$

when the light excitation is terminated. Here n is the density of free charge carriers, τ is the recombination lifetime, γ is the recombination coefficient and β is the effective recombination order which depends on the ratio between dominant recombination mechanisms: $\beta = 1$ for the SRH recombination, $\beta = 2$ for the bipolar recombination and $\beta = 3$ for Auger recombination. From Equation 5 τ can be expressed by:

$$\tau = \frac{n}{U(n)} = \frac{1}{\gamma n^{\beta-1}}. \quad (6)$$

If $\beta > 1$ τ becomes dependent on n and thus, on time. In this case τ is considered as an instantaneous recombination lifetime, which continuously changes its value over time. Assuming that $n \sim \exp(qV_{oc}/kT)$, the relationship between τ and the V_{oc} decay is governed by the following equation in the case of a high excitation level[28, 29]

$$\tau = -\frac{kT}{q}\left(\frac{dV_{oc}}{dt}\right)^{-1}. \quad (7)$$

Figure 5b shows the calculated τ using Equation (7) as a function of time for the control and irradiated solar cells. It can be seen that τ depends on time and thus, on the density of charge carriers. The initial values of the instantaneous recombination lifetimes of the control and irradiated solar cells increase over time and then approaches saturation at about 0.1 ms and 1 ms, respectively. This behaviour indicates the dominance of different recombination mechanisms within different time ranges after the termination of the light excitation. The further increase of τ results due to the low level of excitation condition at low V_{oc}. In this case the system does not fit into the model described by Equation 7 and other approaches should be considered[28] that are not in the scope of this study. The smaller slope of the τ vs. time dependence during first few microseconds may be due to the presence of fast traps in the perovskite layers. The release of trapped charge carriers partially compensates recombination losses just after the termination of the light. The initial value of τ in the control solar cell is slightly larger than that in the irradiated solar cell but this is caused by a large

difference in the density of free charge carriers in these devices under the same illumination conditions. A correct comparison between the two devices can be carried out when τ is plotted as a function of V_{oc} (**Figure 5c**). The density of free charge carriers $n \sim \exp(qV_{oc}/kT)$. It is more convenient to compare recombination lifetimes in the control and irradiated solar cells at the same V_{oc} value and thus, at the same density of free charge carriers. It can be clearly seen that the recombination lifetime in the irradiated solar cell is significantly larger than that in the control solar cell at the same V_{oc}. The next step is to determine the dominant recombination mechanisms and estimate their relative contribution to the total recombination losses.

The effective recombination order β can be determined from Equation (6) and is given by:

$$\beta = 1 + \frac{d \ln \tau^{-1}}{d \ln n}. \tag{8}$$

Taking into account the mentioned exponential relationship between n and V_{oc}, Equation 8 can be rewritten in a more practical form:[29]

$$\beta = 1 + \frac{kT}{q} \frac{d \ln \tau^{-1}}{dV_{oc}}. \tag{9}$$

Figure 5d shows the β vs. V_{oc} dependences for devices 1 and 2, as calculated from the τ vs. V_{oc} dependences (Figure 5c) using Equation 9. Four different regions have to be considered in Figure5d. During the first few microseconds β increases due to the release of charge carriers from the fast traps in both devices (at high V_{oc}). Then, β for the control solar cell reaches its maximum at a slightly lower value than 2. This indicates the dominance of the bipolar recombination with a noticeable contribution from the SRH recombination since $\beta < 2$. For the irradiated solar cell β also reaches its maximum but its value is slightly larger than 2. This is due to a smaller relative contribution from the SRH recombination, which correlates with the V_{oc} vs. light intensity dependences, shown in Figure4b, and a slight contribution from the Auger recombination. A small contribution from the Auger recombination is possible since

the irradiated solar cell possesses a larger V_{oc} and thus, a much larger density of free charge carriers.[30-32]

The net rates of the bipolar and SRH recombination can be given as follows by $U_{BPR} = \gamma_{BPR} n^2$ and $U_{SRH} = \gamma_{SRH} n$, respectively. The ratio between the recombination rates U_{SRH}/U_{BPR} is governed by:

$$\frac{U_{SRH}}{U_{BPR}} = \frac{\gamma_{SRH}}{\gamma_{BPR}} n^{-1} \propto \frac{\gamma_{SRH}}{\gamma_{BPR}} \exp\left(-\frac{qV_{oc}}{kT}\right) \quad (10)$$

According to Equation 10 the relative contribution of the SRH recombination exponentially increases with the decrease of V_{oc}. This trend is well seen in the third region in Figure5d where β abruptly decreases almost to unity with the further decay of V_{oc}. The SRH recombination dominates within the third region for both devices ($\beta \approx 1$). The forth region in Figure5d is characterized by an increase of the coefficient β. As mentioned earlier, this behavior is caused by the low excitation level at low V_{oc}. It should be noted that the steady state and transient photoelectrical characteristics of both solar cells provide evidence of reduced non-radiative SRH recombination losses in the irradiated solar cell that results in the increase of V_{oc} and τ. This finding correlates well with the analysis of the DC dark current transport conditions.

3. Discussion

The results presented in the previous section reveal that the control and irradiated solar cells possess different recombination conditions for injected and photo-generated charge carriers. The decrease of the relative contribution of the non-radiative SRH recombination is responsible for the observed V_{oc} and *FF* enhancement in the irradiated solar cells. This experimental result is completely unexpected since it is known that the radiation damage of conventional inorganic semiconductors results in the formation of defects which usually form deep energy levels within the band gap and act as efficient non-radiative recombination

centers. Consequently, losses due to higher non-radiative recombination rate, smaller V_{oc} and lower *FF* should be observed. However, this scenario does not work in perovskite solar cells and the reasons for that are discussed in this section.

Let us first consider the photo-degradation of the control solar cell under standard AM 1.5 illumination. Methylammonium lead iodine perovskite is a hybrid organic-inorganic material and thus, the organic framework suffers from the photo-degradation. The deprotonation and dissociation of CH_3NH_3 molecules to CH_3NH_2, CH_2NH_3, CH_3, NH_3, etc. is possible by the decoupling of C-H, N-H or C-N bounds via interaction with the photo-generated electrons.[33-35] It is shown that the mentioned fragments of CH_3NH_3, located in the perovskite interstitial, and their possible complexes with iodine atoms form deep energy levels in the band gap and considerably increase non-radiative recombination losses.[36] This statement correlates with our experimentally measured DC electrical and photoelectrical properties and AC characteristics of the control solar cell: large values of the ideality coefficient n_1 and the slope of the V_{oc} vs. light intensity dependence (Figure 2a and 4b); small values of the recombination lifetime τ and the effective recombination order β (Figure 5c and 5d). Moreover, recombination centers do not act as doping sources and thus, the high frequency capacitance of the control solar cell is voltage independent, which is characteristic for an intrinsic semiconductor (Figure 3b).

The irradiated solar cell is also affected by the same photo-degradation processes. Additionally the fragmentation of CH_3NH_3 molecules is enhanced by energetic secondary electrons due to the proton bombardment. However, high energy protons also influence the inorganic Pb-I framework of perovskite by the formation of Frenkel defects. These point defects are formed when an atom leaves its place in the lattice, creating a vacancy and an interstitial in a nearby location; e.g.: an iodine vacancy V_I and the displaced interstitial I_i, and a lead vacancy V_{Pb} and the corresponding interstitial Pb_i. Taking into account the difference in the number of atoms (three iodine atoms per one lead atom) and in atomic masses of lead and

iodine atoms it is conceivable that the density of V_I and I_i will be larger than that of V_{Pb} and Pb_i in the analogy with InP where the radiation damage is mainly associated with the displacement of light weight phosphorus atoms.[2, 37]

Due to the ionic bounding nature of perovskite and its large dielectric constant the point defects V_I, I_i and V_{Pb} form shallow traps with energy levels close to the conduction or valance bands.[22, 38] This unique feature of hybrid organic-inorganic perovskites is the main reason why solution processed perovskite films with low structural perfection and many intrinsic defects possess a large diffusion length of photo-generated charge carriers and show extraordinary photovoltaic parameters. These shallow levels do not participate in the non-radiative recombination according to the SRH statistics but they act as doping sources which are responsible for unintentional doping of perovskites.[22] This is consistent with the observed Mott-Schottky dependence in the irradiated solar cell (Figure 3c). The simultaneous existence of donor- and acceptor-type shallow energy levels formed by point defects and deep energy levels formed by interstitial fragments of CH_3NH_3 result in self-compensation. Thus, the photo-degraded and proton irradiated perovskite should be considered as a partially compensated semiconductor.[15, 39-41] Moreover, the proton induced point defects and fragments of CH_3NH_3 may also form defect related complexes.[42, 43] It is possible that these complex defects do not participate in recombination processes. For instance, this mechanism of a high radiation hardness is realized in InP. As mentioned earlier, it was established that a dominant defect, produced by high energy electron or proton irradiation, in InP is associated with phosphorous vacancies V_P, which acts as an efficient recombination center. However, under illumination or after low temperature annealing this defect transforms to a defect with no recombination activity. This transformation should be associated with the formation of a complex between V_P and doping impurities since the radiation hardness of InP increases with the doping concentration.[2, 37]

Therefore, a partial compensation of deep traps, originated from the photo-degradation of CH_3NH_3 molecules, or their participation in the formation of recombination non-active defect complexes with proton-induced Frenkel defects reduces non-radiative recombination losses in the perovskite active layer. This is a reason for the unexpectedly observed enhancement of main photoelectric parameters V_{oc}, *FF* and τ of the proton irradiated perovskite solar cell in comparison to the control solar cell.

4. Conclusions

We have carried out a complex analysis and comparison of the device physics of perovskite solar cells with and without high energy (68 eV) proton irradiation with a total dose of 10^{13} protons cm^{-2} in combination with white light illumination. Dark J-V curves showed that the proton treatment does not change properties of the hole and electron collecting contacts. However, the shunt resistance of the control solar cell is significantly smaller in comparison to the irradiated solar cell due to the dominance of the Sah–Noyce–Shockley recombination current transport mechanism.

Dark capacitance characteristics provide evidence that the dielectric constants of the PCBM and perovskite layers are immune to proton irradiation. The irradiated solar cell, in the contrary to the control solar cell, shows voltage dependence of its high frequency capacitance indicating the presence of doping sources in the perovskite layer. The estimated density of proton induced uncompensated doping centers amounts to $N = 4.8\times10^{15}$ cm^{-3}.

The presence of the both bipolar and SRH recombination mechanisms is noticed in the control and irradiated solar cells from V_{oc} vs. light intensity dependences and V_{oc} decay measurements. A relative contribution of the non-radiative SRH recombination to the total recombination losses was shown by the both techniques to be larger in the control solar cell.

Taking into account the simultaneous photo-degradation of the organic methylammonium framework and the proton-induced point defects in the inorganic Pb-I

framework the perovskite active layer in the irradiated solar cell should be considered as a partially compensated semiconductor. Deep energy levels, formed by the photo-induced deprotonation and dissociation of methylammonium molecules are partially compensated by proton induced point defects, which create shallow energy levels only. While photo-induced degradation is present in any perovskite solar cell, this causes the observed attenuation of the non-radiative SRH recombination losses and the enhancement of main photoelectric parameters of proton irradiated solar cells.

The obtained nontrivial results are very promising for the developing of low-cost, thin film and radiation resistant perovskite solar cells or other electronic and sensor devices for applications under harsh radiation conditions.

5. Experimental section

Preparation of the perovskite solar cells

Inverted perovskite solar cells were prepared following the layer sequence glass/ITO/PEDOT:PSS/$CH_3NH_3PbI_3$/$PC_{61}BM$/PCB/Ag. A 60 nm thick PEDOT:PSS (Heraeus PH 4083) film was spin-coated on glass/ITO at 3000 rpm for 30 s and annealed at 150°C for 20 min. Afterwards a stoichiometric $CH_3NH_3PbI_3$ precursor solution containing 1.1 M of PbI_2 and CH_3NH_3I was prepared in a mixed solvent of γ- butyrolactone and dimethyl sulfoxide with a volume ratio of 70 vol.% to 30 vol.%. The $CH_3NH_3PbI_3$ solution was spin-coated with the following sequence: 1000 rpm for 10 s, 2000 rpm for 20 s, and 5000 rpm for 20 s. At the last stage 150 µl toluene were dripped on top of the $CH_3NH_3PbI_3$ layer. Subsequently, the $CH_3NH_3PbI_3$ layer was crystallized at 100 °C for 10 minutes. The absorber had a thickness of about 350 nm. The electron selective contact was formed by spin-coating a 50 nm thick $PC_{61}BM$ layer at 2500 rpm for 60 s. After short annealing (100°C, 10 min) a thin layer of bathocuproine (BCP) was spin-coated at 4000 rpm (0.5 mg/ml, ethanol). Afterwards, the devices were transferred from inert atmosphere into an evaporation chamber with residual

pressure of 10^{-7} mbar. Ag contacts (100 nm) were thermally evaporated using a shadow mask. The overlap of the patterned ITO and the metal contacts defined the active area of the solar cells and amounted to 0.16 cm^2.

Proton irradiation

The proton irradiation experiments were performed at the cyclotron of the Helmholtz-Zentrum Berlin. The proton energy was 68 MeV. The Tandetron-cyclotron combination provides a high stability of the beam intensity. To achieve a homogeneous irradiation over an area of 3.0 cm^2 wobbler magnets were used. The beam intensity was monitored online using a transmission ionization chamber from 'PTW Freiburg GmbH'. The proton flux was kept constant at around $\varphi = 1.68\times10^9$ p cm^{-2} s^{-1}. The accumulated total dose was 1.02×10^{13} p cm^{-2}.

Characterization

The perovskite solar cells were characterized using an AM1.5G simulated solar spectrum (Newport LCS-100 class ABB sun simulator). The light intensity was calibrated by means of a calibrated Si photodiode (Fraunhofer ISE CalLab PV Cells). Because of the well-known hysteresis effect current-voltage scans were performed in forward and reverse direction using a voltage sweep of 85 mV/s. Different light intensities were obtained by using neutral filters with different optical density. The EQE was measured without bias voltage and illumination.

The spectral distributions of the real and imaginary components of the impedance of the solar cells were measured by an impedance analyser HP 4192A in the dark at different DC biases and room temperature. The small amplitude AC signal (10 mV) was applied to prevent the effect of the AC signal on the measured impedance.

The V_{oc} decay measurements were carried out under 100 mW cm^{-2} light excitation provided by a fast switching blue (465-470 nm) LED light source. The light source is

governed by a fast switching driver and a square wave function generator. The switch-off time of the light source was measured to be less than 30 ns. The solar cells were connected to the input of a digital oscilloscope PicoScope 5244B via a high impedance buffer (5GΩ) with the bandwidths of 200 MHz each.

Acknowledgements

V.V.B. acknowledges the Alexander-von-Humboldt Foundation for financial support in the framework of the Georg Forster Research Fellowship.

Received: ((will be filled in by the editorial staff))
Revised: ((will be filled in by the editorial staff))
Published online: ((will be filled in by the editorial staff))

[1] F. C. Treble, *Microelectronics Reliability* **1962**, *1*, 299.
[2] T. Markvart, *J. Mater. Sci. Mater. Electron.* **1990**, *1*, 1.
[3] K. Otte, L. Makhova, A. Braun, I. Konovalov, *Thin Solid Films* **2006**, *511-512*, 613.
[4] M. Liu, M. B. Johnston,H. J. Snaith, *Nature* **2013**, *501*, 395.
[5] C. S. Ponseca, T. J. Savenije,M. Abdellah, K. Zheng, A. Yartsev, T. Pascher, T. Harlang, P. Chabera, T. Pullerits, A. Stepanov, J.-P. Wolf, V. Sundstrom, *JACS* **2014**, *136*, 5189.
[6] M. Coll, A. Gomez, E. Mas-Marza, O. Almora, G. Garcia-Belmonte, M. Campoy-Quiles, J. Bisquert, *J. Phys. Chem. Lett.* **2015,** *6*, 1408.
[7] Z. Xiao, J. Huang, *Adv. Electron. Mater.* **2016**, *2*, 1600100.
[8] Research Cell Efficiencies. *http://www.nrel.gov/ncpv/images/efficiency_chart.jpg*.
[9] F. Lang, N. H. Nickel, J. Bundesmann, S. Seidel, A. Denker, S. Albrecht, V. V. Brus, J. Rappich, B. Rech, G. Landi, H. C. Neitzert, *Adv. Mater.* **2016**, DOI: 10.1002/adma.201603326.
[10] H.C. Neitzert, M. Ferrara, M.M. Kunst, A. Denker, Z. Kertesz, B. Limata, L. Gialanella, M. Romano, *Phys. Stat. Sol. B* **2008**, *245*, 1877.
[11] V.V. Brus, A. K. K. Kyaw, P. D. Maryanchuk, J. Zhang, *Prog. Photovolt.: Res. Appl.* **2015**, *23*, 1526.
[12] C.-J. A. H. Wetzelaer, M. Scheepers, A. M. Sempere, C. Momblona, J. Avila, H. J. Bolink, *Adv. Mater.* **2015**, *27*, 1837.
[13] S. M. Sze, K. K. Ng, *Physics of Semiconductor Devices*, Wiley, NJ, USA **2007**.
[14] C.-T. Sah, R. N. Noyce, W. Schockley, *IRE* **1957**, *45*,1228.
[15] L. A. Kosyachenko, *Semiconductors* **2006**, *40*, 710.
[16] V. V. Brus, *Semicond. Sci. Technol.* **2012**, *27*, 035024.
[17] V.V. Brus, C.M. Proctor, N.A. Ran, T.-Q. Nguyen, *Adv. Energy Mater.* **2016**, *6*,1502250.
[18] I. Balberg, E. Gal, *J. Appl. Phys.* **1985**, *58*, 2617.
[19] J. Bisquert, L. Bertoluzzi, I. Mora-Sero, G. Garcia-Belmonte, *J. Phys. Chem. C* **2014**, *118*, 18983.
[20] J. D. Jackson, *Classical Electrodynamics*, Wiley, New York, USA **1999**.
[21] F. Jahani, S. Torabi, R. C. Chiechi, L. J. A. Kister, J. C. Hummelen, *Chem. Commun.* **2014**, *50*, 10645.
[22] J. Kim, S.-H. Lee, J. H. Lee, Ki-Ha Hong, *J. Phys. Chem. Lett.* **2014**, *5*, 1312.
[23] J. P. Donnelly, A. G. Milnes, *IEEE Trans. Electron Devices* **1967**, *ED-14*, 63.
[24] E. F. Bartusiak, J. Becher, *Appl. Optics* **1979**, *18*, 3342.
[25] L. J. A. Koster, V. D. Mihailetchi, R. Ramaker, P. W. M. Blom, *Appl. Phys. Lett.* **2005**, *86*, 123509.
[26] S. R. Cowan, A. Roy, A. J. Heeger, *Phys. Rev. B* **2010**, *82*, 245207.
[27] S. R. Cowan, W. L. Leong, N. Banerji, G. Dennler, A. J. Heeger, *Adv. Funct. Mater.*, **2011**, *21*, 3083.
[28] J. E. Mahan, T. W. Ekstedt, R. I. Frank, R. Kaplow, *IEEE Trans. Electron Devices* **1979**, *ED-26*, 733.
[29] A. Zaban, M. Greenshtein, J. Bisquert, *ChemPhysChem* **2003**, *4*, 859.
[30] M. J. Kerr, A. Cuevas, *J. Appl. Phys.* **2002**, *91*, 2473.

[31] Y. C. Shen, G. O. Mueller, S. Watanabe, N. F. Gardner, A. Munkholm, M. R. Krames, *Appl. Phys. Lett.* **2007**, *91*, 141101.
[32] G. Xing, N. Mathews, S. Sun, S. S. Lim, Y. M. Lam, M. Gratzel, S. Mhaisalkar, T. Ch. Sum, *Science* **2013**, *342*, 344.
[33] C. H. Peters, I. T. Sachs-Quintana, W. R. Mateker, T. Heumueller, J. Rivnay, R. Noriega, Z. M. Beiley, E. T. Hoke, A. Salleo, M. D. McGehee *Adv. Mater.* **2012**, *24*, 663.
[34] R. A. Street, J. E. Northrup, B. S. Krusor, *Phys. Rev. B* **2012**, *85*, 205211.
[35] N. H. Nickel, F. Lang, V. V. Brus, J. Rappich, *submitted*.
[36] P. Delugas, A. Filippetti, A. Mattoni, *Phys. Rev. B* **2015**, *92*, 045301.
[37] M. Yamaguchi, K. Ando, *J. Appl. Phys.* **1988**, *63*, 5555.
[38] W.-J. Yin, T. Shi, Y. Yan, *Appl. Phys. Lett.* **2014**, *104*, 063903.
[39] T. Kamiya, E. Wagner, *J. Appl. Phys.* **1977**, *48*, 1928.
[40] G. Mandel, *Phys. Rev.* **1964**, *134*, A1073.
[41] D. C. Look, K. D. Leedy, L. Vines, B. G. Svensson, A. Zubiaga, F. Tuomisto, D. R. Doutt, L. J. Brillson, *Phys. Rev. B* **2011**, *84*, 115202.
[42] M.-H. Du, H. Takenaka, D. J. Singh, *J. Appl. Phys.* **2008**, *104*, 093521.
[43] M. Kumar, A. Dubey, N. Adhikari, S. Venkatesan, Q. Qiao, *Energy Environ. Sci.* **2015**, *8*, 3134.

TOC entry

The enhancement of open-circuit voltage, fill factor and recombination lifetime is shown in photo-degraded and high energy proton irradiated $CH_3CN_3PbI_3$ perovskite solar cells. These enhancements result from lower non-radiative recombination losses in the proton irradiated devices. A reasonable mechanistic basis of the observed decrease of non-radiative recombination losses can be explained by the compensation of deep traps originated from the photo-degradation of methylammonium molecules by proton induced Frenkel defects in the inorganic Pb-I framework.

Keywords: perovskite, photo-degradation, proton irradiation, compensation

Viktor V. Brus[*]*, Felix Lang, Jürgen Bundesmann, Sophie Seidel, Andrea Denker, Bernd Rech, Giovanni Landi, Heinrich C Neitzert, Jörg Rappich and Norbert H. Nickel*

Defect Dynamics in Proton Irradiated $CH_3NH_3PbI_3$ Perovskite Solar Cells